JOURNAL OF MATERIALS SCIENCE **35** (2000) 3889–3902

Crystal structure of barium titanate fine particles including Mg and analysis of their lattice vibration

S. WADA, M. YANO, T. SUZUKI, T. NOMA
Department of Applied Chemistry, Tokyo University of Agriculture and Technology, 24-16 Nakamachi 2-chome, Koganei, Tokyo 184-8588, Japan
E-mail: swada@cc.tuat.ac.jp

Fine barium titanate crystallites with various Mg contents were prepared by a hydrothermal method. These particles were spherical single crystallites with an average size of about 63 nm, regardless of Mg contents from 0 to about 0.15 wt%. It was confirmed that Mg replaced substitutionally on Ti site. On the refinement of the crystal structure with a Rietveld method, the crystal structure of the particles without Mg was tetragonal with a tetragonality of 1.0015 while those including Mg approached from tetragonal to cubic gradually with increasing Mg content. On the other hand, a Raman measurement indicated that the local structure remained tetragonal regardless of Mg contents. Moreover, the resonance frequency for each phonon mode was independent of Mg contents while their damping factor increased with increasing Mg content, which suggested that state of the phonon became more unstable with increasing Mg content. Therefore, the lattice defects induced by Mg into the barium titanate particles can give the phonon a similar effect to that of temperature in barium titanate single crystal.

1. Introduction

It is well known that as factors, which can cause a structural phase transition of displacive-type ferroelectrics such as $PbTiO_3$ and $BaTiO_3$, there are temperature, [1–5] pressure, [6] particle size, [7, 8] grain size [9] and domain size [10]. Among the above factors, it confirmed experimentally that some factors, e.g., temperature, [1, 2] pressure [6] and particle size, [7] can affect a stability of phonon, especially stability of soft mode, and then the structural phase transition caused by the change of these factors has explained with the soft mode theory [11–14].

Recently, some investigators reported that lattice hydroxyl group included in $BaTiO_3$ fine particles prepared by a hydrothermal method could make its crystal structure an expanded cubic [15–17]. Hennings and Schreinemacher found that in hydrothermal $BaTiO_3$ fine particles, a cubic phase transformed gradually into a tetragonal phase with decreasing concentration of the lattice hydroxyl group under a constant particle size of about 200 nm [16]. Wada *et al.* also confirmed this phenomenon in hydrothermal $BaTiO_3$ fine particles with particle sizes from 20 to 100 nm [18]. The above results showed that the lattice hydroxyl group can also affect the structural phase transition of perovskite-type ferroelectrics, as well as temperature, pressure, particle size, grain size and domain size.

In order to explain the above phenomenon, Wada *et al.* proposed a new model that the lattice hydroxyl group can affect the stability of phonon [19]. Using this model, the state of phonon becomes unstable with increasing concentration of the lattice hydroxyl group, and thus, the crystal structure changed from tetragonal to cubic gradually. Moreover, they also analyzed the state of phonon from IR reflection spectra using Four Parameter Semi-Quantum model, and revealed that only a damping factor increased with increasing concentration of the lattice hydroxyl group while a resonance frequency is almost constant regardless of its concentration [20]. This result supported the availability of their model concerning lattice hydroxyl group. It, however, is doubtful whether this model can be applied on the case of other lattice defects except for lattice hydroxyl group. Thus, it is very important to investigate an effect of other lattice defects except for lattice hydroxyl group on phonon and crystal structure of $BaTiO_3$ fine particles.

In this study, we try to induce a lattice defect on Ti site. This is because the soft mode of $BaTiO_3$ is Slater mode (=stretching vibration between Ti and O_6 octahedra), and the defect on Ti site can significantly affect the soft mode. For this purpose, the addition of Mg into $BaTiO_3$ fine particles was chosen. This is because (1) ionic radius of Mg^{2+} (0.065 nm) is similar to that of Ti^{4+} (0.068 nm), and (2) in $BaTiO_3$ ceramics, it was reported that a Mg ion replaced substitutionally on Ti site [21]. Thus, we prepare $BaTiO_3$ fine particles including various Mg contents by a hydrothermal method, and investigate their crystal structure using XRD and Raman measurements and the states of their phonon using Raman and far-infrared measurements. Moreover, we discuss a dependence of the crystal structure and the state of phonon on Mg contents, and describe about relationship between lattice defect and phonon.

2. Experimental

$BaTiO_3$ fine particles including various Mg contents were prepared by a hydrothermal method using titanium tetrahydroxide $Ti(OH)_4$, magnesium dihydroxide $Mg(OH)_2$ and barium dihydroxide $Ba(OH)_2{\cdot}8H_2O$. After dissolution of titanium tetrachloride and magnesium dichloride in cooled water below 10 °C at various Mg/Ti atomic ratios from 0 to 0.25, aqueous ammonia was added slowly to this solution below 10 °C, and then a mixed gel of $Ti(OH)_4$ and $Mg(OH)_2$ was formed. Ammonium and chloride ions in this gel solution were mostly removed by repeated decantation (about 15 times), and the gel solution was used as a B-site source. After the addition of $Ba(OH)_2{\cdot}8H_2O$ to the gel solution at a constant Ba/(Ti + Mg) atomic ratio of 2, the mixed solution was stirred in a conventional autoclave at 150 °C for 4 h, and then $BaTiO_3$ particles were formed. These particles were filtered, washed and then stirred in acetic acid solution (6 mol/dm^3) at 50 °C for 1 h, in order to remove unfavorable $Ba(OH)_2$, $BaCO_3$ and $Mg(OH)_2$. After the acetic acid treatment, the particles were filtered, washed, dried under vacuum at 80 °C for 16 h. The particles were calcined at 800 °C for 1 h to remove hydroxyl group included in the particles, and used as the samples.

The crystal structure and the phonon of these particles were investigated at room temperature using a powder X-ray diffractometer (XRD) (RAD-2C, Rigaku, Cu-K_α, 30 kV, 20 mA, and MXP18HF22/SRA, Mac Science, Cu-K_α, 45 kV, 200 mA), a Fourier transform infrared spectrometer (FT-IR) (JIR-100, JEOL, 32 scans, 4000–400 cm^{-1}), a Fourier transform far-infrared spectrometer (FT-FIR) (SPECTRUM 2000, Perkin Elmer, 600 scans, 700–50 cm^{-1}), and a Fourier transform Raman scattering spectrometer (Raman) (SYSTEM 2000R FT-RAMAN [DPY], Perkin Elmer, 1064 nm, 100 mW, 50 scans, 4000–200 cm^{-1}). The impurity included in the particles was examined using FT-IR and a differential thermal analysis with thermogravimetry (TG-DTA) (TG-DTA2000, Mac Science). The average particle sizes were estimated using a transmission electron microscope (H-700H, Hitachi, 200 kV). Contents of Ba,Ti and Mg included in the particles were measured by an atomic absorption (AA) (170-30 type, Hitachi) and a ICP-MS spectrometry (ICP-MS) (HP4500, Yokogawa). Impedance in the compacts of the particles was measured at room temperature using a LF impedance analyzer (HP4192A, Hewlett Packard, 5 Hz–13 MHz) in a four terminal pair configuration.

3. Results

3.1. Impurity and particle size

To investigate kinds and amount of the impurity included in the particles, the measurements using FT-IR and TG-DTA were done. As the results, there exists only hydroxyl group, except for Mg, as a impurity in all as-prepared particles, and amount of hydroxyl group (about 2.4 ± 0.5 wt% as H_2O) was almost constant regardless of Mg contents. Moreover, the most of hydroxyl group desorbed below 600 °C, and above 600 °C there was no weight loss. Previously, we reported that in hydrothermal pure $BaTiO_3$ particles, a crystal structure changed from cubic to tetragonal with desorbing lattice hydroxyl group and at the same time, a state of phonon became more stable, which revealed that the effects of lattice hydroxyl group on the crystal structure and the phonon of $BaTiO_3$ particles were very significant [16–20]. In order to investigate precisely an effect of Mg on the crystal structure and the phonon, it is most important to remove completely lattice hydroxyl group included in the particles. Therefore, all particles were calcined at 800 °C for 1 h, and then it was confirmed that there was no impurity, except for Mg, in all particles treated at 800 °C from FT-IR and TG-DTA measurements. Through this manuscript, we will characterize about the particles treated at 800 °C.

To estimate Mg content in the above particles, the measurements using AA and ICP-MS were done. The hydrothermal $BaTiO_3$ particles were dissolved completely into concentrated hydrochloric acid above 150 °C, and adjusted to proper concentrations of Ba, Ti and Mg from 0.01 to 10 ppm using HCl(1 + 1) solution for the measurement. Fig. 1 shows a relationship between Mg content included in the particles and Mg/Ti atomic ratio in starting materials estimated from AA measurement. In this study, we defined a Mg content as a percentage by weight of Mg. Mg content increased with increasing Mg/Ti atomic ratio in starting materials below Mg/Ti atomic ratio of 0.1, and became almost constant around 0.15 wt% above Mg/Ti atomic ratio of 0.1 in starting materials. In the hydrothermal method, a obtained product is the one with the lowest free energy for its formation under some conditions such as temperature, pressure and kinds and amount of the starting materials. This result suggested that the maximum of Mg content in solid solution of MgO-$BaTiO_3$ system under the condition used in this study was about 0.15 wt%. Thus, we could prepare the samples with various Mg contents from 0 to 0.15 wt%. ICP-MS also showed the

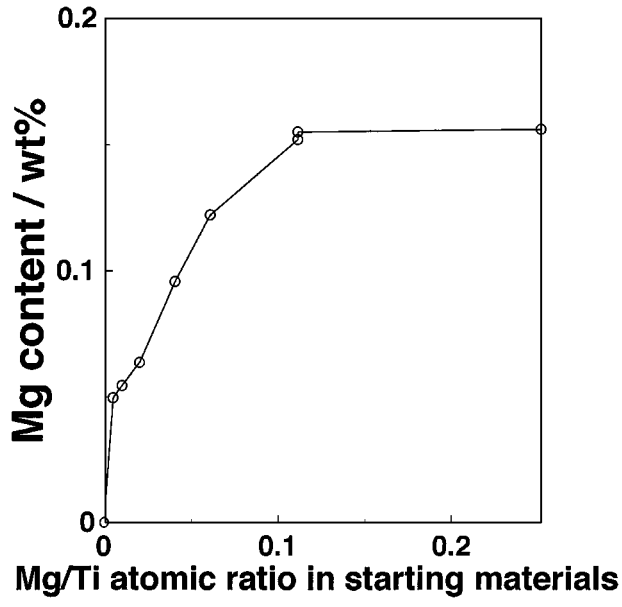

Figure 1 The dependence of Mg contents in hydrothermal $BaTiO_3$ particles on Mg/Ti atomic ratio in starting materials estimated from AA measurements.

TABLE I Each percentage by weight of Ba, Ti and Mg measured using AA and ICP-MS

Sample No.	Ba/wt%	Ti/wt%	Mg/wt%
1	53.3	20.9	0
2	54.5	21.9	0.0495
3	52.5	22.7	0.0543
4	51.5	22.3	0.0634
5	52.3	18.9	0.0956
6	52.2	18.2	0.122
7	54.5	19.1	0.152
8	53.6	18.7	0.155
9	51.9	17.9	0.156

similar results to the AA measurements concerning Mg contents.

Table I shows each percentage by weight of Ba,Ti and Mg measured using AA and ICP-MS. If there is no defect in a $BaTiO_3$ particle, the percentages of Ba and Ti can become 57.88 wt% and 20.54 wt%, respectively. But in Table I, the percentage of Ba was less than ideal one, and was almost constant around 53.0 ± 1.5 wt% regardless of Mg contents. On the other hand, the percentage of Ti decreased with increasing weight percentage of Mg. This result suggested a possibility that the most of Mg can exist substitutionally in Ti site of a $BaTiO_3$ lattice.

Thus, in order to confirm whether Mg exists really in a $BaTiO_3$ lattice or exists as second phase except for $BaTiO_3$, XRD and TEM measurements were performed. From a XRD measurement, all as-prepared hydrothermal particles and all particles calcined at 800 °C for 1 h were assigned to $BaTiO_3$ single phase despite Mg contents. Fig. 2 shows a TEM bright-field image (a), a dark-field image (b), and a selected-area electron diffraction (SAED) pattern (c) of the particles including Mg of 0.155 wt%. The SAED pattern (Fig. 1c) indicates that one particle is a $BaTiO_3$ single crystal, but it was very difficult to determine from this SAED pattern whether its crystal structure can be assigned to cubic or tetragonal with a tetragonality near 1.0. A particle size in the bright-field image were in a good agreement with that in the dark-field image, which also confirmed that one particle was a $BaTiO_3$ single crystal. In the particles including other Mg contents (0–0.152 and 0.156 wt%), we could obtain almost similar results. Thus, the above results revealed that Mg did not exist as the second phase except for $BaTiO_3$ in the particles, and can exist substitutionally in a $BaTiO_3$ lattice. On the basis of the above results, we think that in the hydrothermal $BaTiO_3$ particles prepared at 150 °C, a solubility of Mg into $BaTiO_3$ is about 0.15 wt%.

Moreover, the average particle sizes were estimated using 200–250 particles in TEM bright-field images. Fig. 3 shows dependence of average particle size on Mg content. In the particles without Mg, the average particle size was 62.5 ± 6.7 nm, while that in the particles including Mg of 0.155 wt% was 63.1 ± 6.7 nm. This result indicated that average particle sizes, i.e., crystallite sizes, were almost constant around 63 nm despite Mg contents.

The above results showed that Mg ion could exist substitutionally in a $BaTiO_3$ lattice, but we must clear whether Mg can exist on Ba or Ti site. Thus, to clear the site where Mg replaced, impedance of the particles was measured. The particles were pressed into compacts by a hand-pressing, then pressed them by a cold isostatic

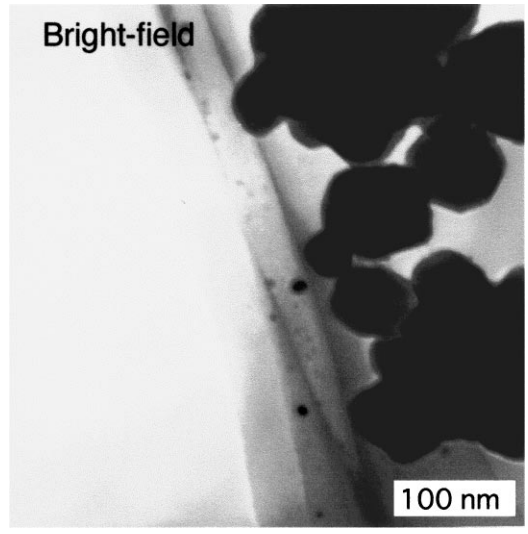

(a)

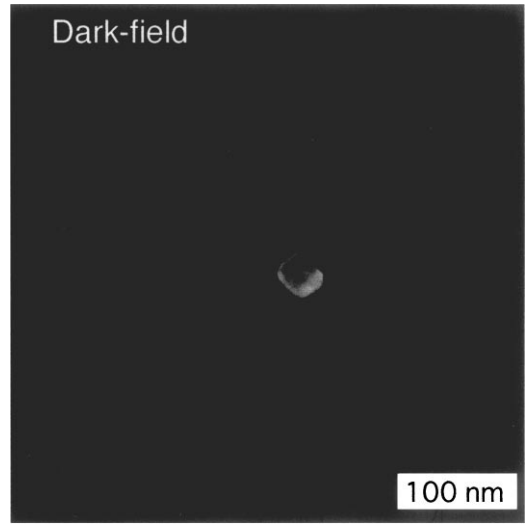

(b)

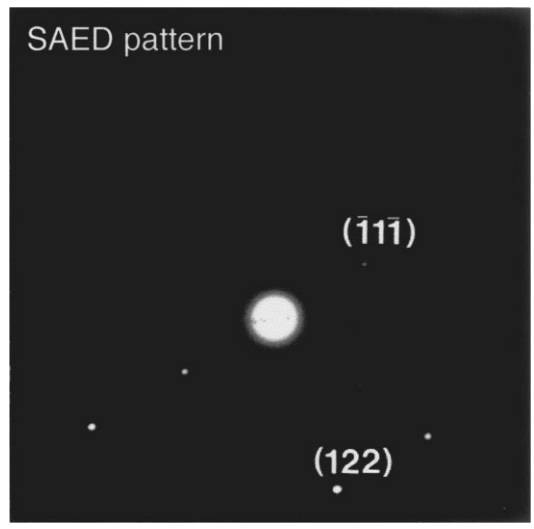

(c)

Figure 2 A TEM bright-field image (a), a dark-field image (b), and a selected-area electron diffraction (SAED) pattern (c) of fine $BaTiO_3$ particles with Mg content of 0.155 wt%.

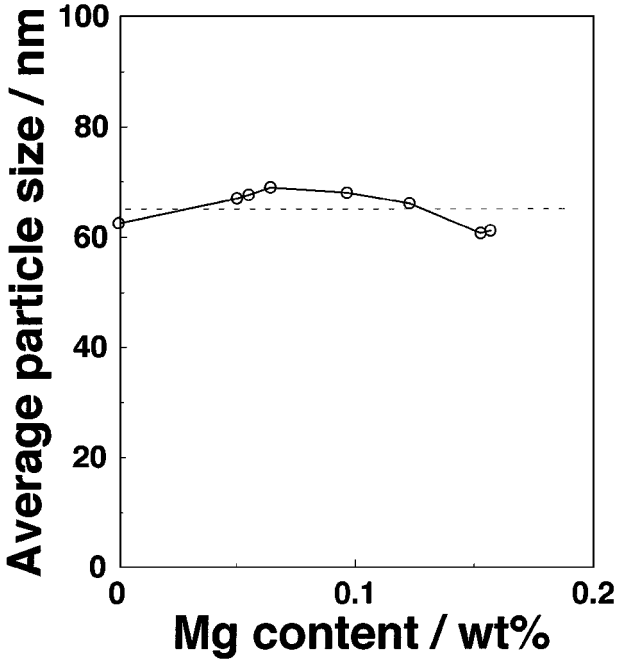

Figure 3 The dependence of average particle size on Mg contents in hydrothermal $BaTiO_3$ particles.

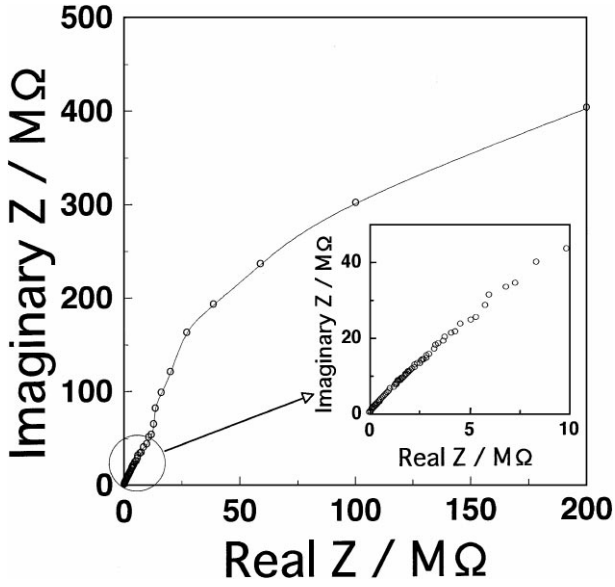

Figure 4 A Cole-Cole plot of impedance ($Z = R - iX$, R: resistance, X: reactance) measured in the compact of hydrothermal $BaTiO_3$ particles including Mg content of 0.155 wt%.

pressing (=CIP) method at 157 MPa for 5 min, and used as the samples for the impedance measurements. Fig. 4 shows a Cole-Cole plot of impedance ($Z = R - iX$, R: resistance, X: reactance) measured at room temperature in the compact of the particles including Mg of 0.155 wt% as a typical example. In Fig. 4, there were two partially overlapping semicircles, i.e., (1) a very small semicircle toward lower resistance (0–10 MΩ) and (2) a very large one toward higher resistance (>10 MΩ). In complete impedance diagram of the typical ceramics composed of intragrain, grain boundary and electrode, it was reported that a semicircle toward lowest resistance can be assigned to that of intragrain, one at middle assigned to grain boundary, and one toward highest assigned to electrode [22]. On the basis of this report, a semicircle toward lower resistance in Fig. 4 was assigned to that of intraparticle and one toward higher resistance was assigned to that of interface between the particles. Moreover, it can be expected that a resistance of interface between the particles becomes much larger. This is because the samples were compacts of the particles and a contact area between the particles became very small. Therefore, we can consider that a very large semicircle toward higher resistance in Fig. 4 can be assigned to that of interface between the particles.

In the impedance diagrams of the compacts including other Mg contents, the scale of a semicircle toward higher resistance was almost constant regardless of Mg contents, but that of one toward lower resistance decreased with increasing Mg content. In order to estimate resistance of each part, the Cole-Cole plots must be separated completely into two semicircles. However, in this study it was very difficult to separate precisely two semicircles by a calculation. This is because the magnitude of a semicircle assigned to intraparticle was much smaller than that assigned to interface between the particles. Thus, instead of an estimation of semicircle resistance in an intraparticle part, we used the reactance at various resistance in the intraparticle part as a scale of its resistance.

Fig. 5 shows the dependence of the reactance at various resistance (0.5–8 MΩ) on Mg content, which all values in Fig. 5 were obtained from Cole-Cole plots of the compacts, as shown in Fig. 4. Each reactance decreased with increasing Mg content below Mg content of about 0.06 wt%, and above Mg content of about 0.06 wt%, each reactance was almost independent of Mg contents. This suggested that an electrical resistance of the intraparticle became smaller with increasing Mg content below Mg content of about 0.06 wt%.

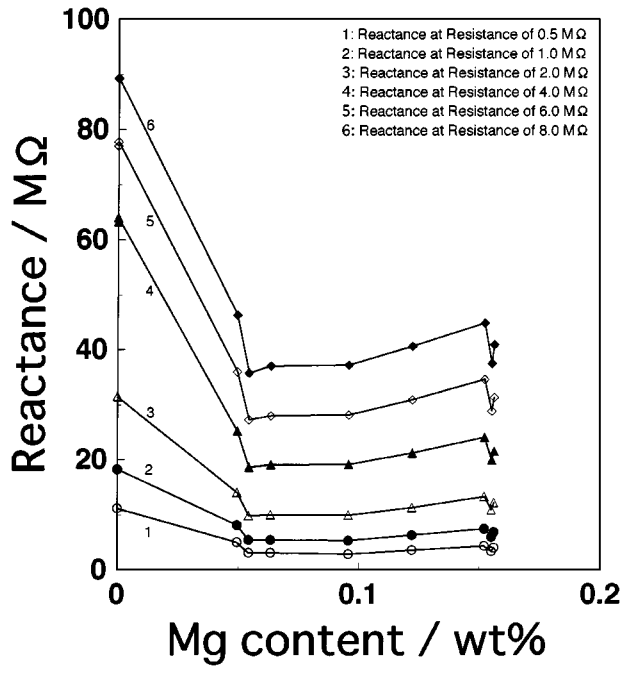

Figure 5 The dependence of reactance at various resistance (0.5–8 MΩ) on Mg content in hydrothermal $BaTiO_3$ particles.

At present, we can not explain why the reactance was almost constant above Mg content of about 0.06 wt%. But, we think that when the resistance of intraparticle became smaller than a certain value, it may be difficult to detect the smaller resistance of intraparticle, since an influence of the resistance of interface between the particles on the Cole-Cole plots was much larger.

If Mg^{2+} ion substitutes Ba^{2+} ion on A site of the $BaTiO_3$ lattice, there is no lattice defect (Mg_{Ba}^{x}) owing to the same charge (2+) of both ions. Thus, we can expect that an electrical resistance is almost constant despite Mg contents. On the other hand, if Mg^{2+} ion substitutes Ti^{4+} ion on B site of $BaTiO_3$ lattice, there exists a lattice defect of Mg_{Ti}'' because of the difference of charge between two ions. Moreover, to satisfy the electroneutrality of the particles, oxygen vacancy $V_O^{\cdot\cdot}$ must be also needed as follows.

$$[Mg_{Ti}''] = [V_O^{\cdot\cdot}] \quad (1)$$

These lattice defects can increase a concentration of carrier contributing to an electric conduction, and thus the electrical resistance must decrease. The results in Fig. 5 indicated that the most of Mg ions can substitute Ti on B site of the $BaTiO_3$ lattice, which also supported those estimated from ICP-MS measurements.

Informations about impurity, particle size and lattice defect in the particles obtained in this study could be given as follows.

(1) As-prepared particles had only hydroxyl group, except for Mg, as impurity, and the amount of hydroxyl group included in the particles was almost constant at about 2.4 wt% as H_2O despite Mg contents.

(2) Most of hydroxyl group desorbed below 600 °C, and the particles treated at 800 °C for 1 h had no impurity.

(3) Mg content included in the particles increased with increasing Mg/Ti atomic ratio in the starting materials, and became constant around 0.15 wt% above a Mg/Ti atomic ratio of 0.1 in the starting materials.

(4) One particle was a $BaTiO_3$ single crystal without second phase, and their average particle sizes were almost constant around 63 nm regardless of Mg contents.

(5) In all particles including Mg, the most of Mg ions substituted Ti ions on B site of the $BaTiO_3$ lattice.

(6) There were two kinds of the lattice defects, i.e., Mg_{Ti}'' and $V_O^{\cdot\cdot}$, in all particles including Mg.

3.2. Crystal structure

Fig. 6 shows a (200) plane of hydrothermal $BaTiO_3$ particles with various Mg contents (0–0.155 wt%) treated at 800 °C for 1 h. A (200) plane of the particles without Mg seems to be one peak, but with increasing Mg content, a (200) plane splitted gradually into two peaks, i.e., a large peak at low 2θ and a small shoulder peak at high 2θ assigned to Cu-$K_{\alpha 1}$ and Cu-$K_{\alpha 2}$, respectively. This result indicated that the crystal structure of the particles approached to normal cubic with increasing Mg contents. Fig. 7 shows the lattice parameter a-axis estimated using α-SiO_2 as an external standard on the assumption that the crystal structure was cubic, and FWHM of a (200) plane on various Mg contents. Their a-axis were almost constant around 0.4005 nm despite Mg contents while FWHM of a (200) plane decreased linearly with increasing Mg content.

Generally, the FWHM of a XRD peak can be determined by three factors, i.e., (a) a crystalline size, (b) a lattice strain and (c) a crystal structure [23]. At first, an effect of the crystalline size can be disregarded since the crystalline sizes were constant regardless of

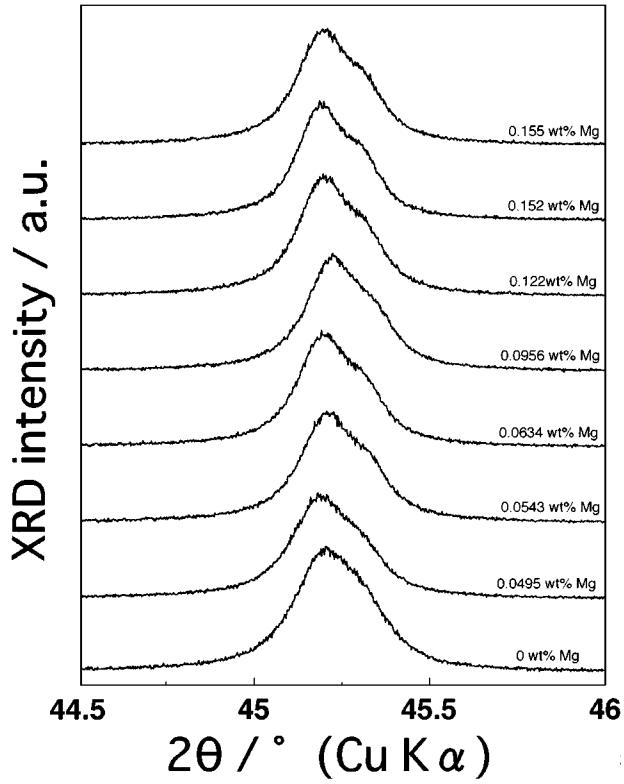

Figure 6 A (200) plane of hydrothermal $BaTiO_3$ particles with various Mg contents treated at 800 °C for 1 h.

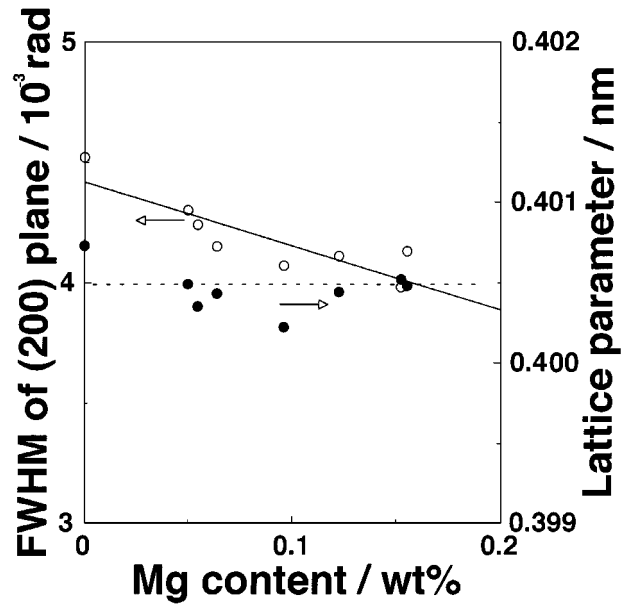

Figure 7 A lattice parameter a-axis on the assumption that the crystal structure was cubic, and FWHM of (200) plane on various Mg contents in hydrothermal $BaTiO_3$ particles.

Mg contents from TEM. Moreover, an influence of the lattice strain also can be neglected. This is because the slopes of lines in Wilson-Hall plots were almost 0 in both the particles including Mg of 0 and 0.155 wt%. Therefore, these results suggested a possibility that the change of FWHM must be caused by a change of the crystal structure.

However, it is very difficult to determine the crystal structure using only peak profile of a (200) plane. Thus, the crystal structure of two kinds of the particles including Mg of 0 and 0.155 wt% were refined using a Rietveld method with a program RIETAN-94 [24]. Table II shows the space group, lattice parameters and the reliable (=R) factor refined in both the particles. Moreover, Tables III–V show the positional parameters refined finally in both the particles. In the particles without Mg, a calculation on the assumption that space group is Pm3m diverged while the calculation on the assumption that space group is P4mm converged at R_{WP} of 8.91. This result indicated that the crystal structure of the particles without Mg was assigned to P4mm (=tetragonal) with a c/a ratio of 1.00154.

On the other hand, the calculation in the particles with Mg of 0.155 wt% was very complicated. On the assumption that a Mg ion can substitute a Ba ion on A site of a $BaTiO_3$ lattice, both the calculation using space groups of Pm3m (=cubic) and P4mm diverged. However, assuming that a Mg ion can substitute a Ti ion of B site of a $BaTiO_3$ lattice, both the calculation using space groups of Pm3m and P4mm converged at R_{WP} of 9.83 and 9.48, respectively. These results supported the results obtained by an ICP-MS and an impedance spectroscopy, which Mg ion replaced Ti ion on B site of the $BaTiO_3$ lattice. Moreover, this also suggested that the crystal structure of the particles including Mg of 0.155 wt% was around the boundary between cubic and tetragonal with a c/a ratio nearer 1.0, which suggested that it is uncertain to clear its space group using a Rietveld method.

Assuming space group of P4mm and the substitution of Mg into Ti site, in the first refinement cycle, the refinement result was not converged to an acceptable level for R factors. Thus, in the next refinement cycle, when the occupation factors and the isotropic thermal parameter of each atom were refined, the refinement result was converged to an almost acceptable level for R factors. However, the occupation factors of Mg, Ti and O(1) refined finally were very doubtful values, as shown in Table IV.

On the other hand, assuming space group of Pm3m and substitution of Mg into Ti site, in the first refinement cycle, the refinement result was converged to an almost acceptable level for R factors. In the result refined finally, only the occupation factor of Mg was relatively large values while the other factors except for the Mg occupation factor were converged to normal values, as shown in Table V. Therefore, we believe that in hydrothermal $BaTiO_3$ particles with Mg of 0.155 wt%, it is suitable to assign its space group into Pm3m.

The above results revealed that the crystal structure observed using XRD changed from tetragonal with a c/a ratio of 1.00154 to cubic with increasing Mg content. In other words, it means that a gradual structural phase transition from tetragonal to cubic occurred with increasing Mg content. Thus, the change of FWHM of a (200) plane in Fig. 6 was caused by the above change of the crystal structure.

However, in Tables IV and V, the occupation factors of Ba, Ti and Mg were different from the values in Table I obtained using AA and ICP-MS. First of all, Mg/Ti atomic ratios calculated using the Rietveld method were much larger than that obtained using AA and ICP-MS. Now, we think that Mg/Ti atomic ratios obtained using AA and ICP-MS were correct, but can not explain this difference between values from two methods.

Fig. 8 shows powder Raman scattering spectra of the hydrothermal $BaTiO_3$ particles with various Mg contents (0–0.155 wt%) treated at 800 °C for 1 h. In the crystallography, Raman-active modes in tetragonal

TABLE II The lattice parameters and the reliable factors for hydrothermal $BaTiO_3$ particles without Mg and with Mg of 0.155 wt%

	No Mg	0.155 wt% Mg	
Space group	P4mm	P4mm	Pm3m
a-axis (nm)	0.400604	0.400641	0.400740
c-axis (nm)	0.401222	0.401054	—
R_{WP} (%)	8.91	9.48	9.83
R_P (%)	5.85	6.00	6.21
R_I (%)	1.59	1.31	0.95
R_F (%)	0.90	0.88	0.78

TABLE III The positional parameters as P4mm for hydrothermal $BaTiO_3$ particles without Mg

	g	x	y	z	B
Ba	0.92	0.0000	0.0000	−0.01255	0.18
Ti	0.90	0.5000	0.5000	0.4865	0.32
O(1)	0.89	0.5000	0.5000	0.003120	0.61
O(2)	1.0	0.5000	0.0000	0.5008	0.57

*g: occupation factor; B (Å^2): Isotropic thermal parameter.

TABLE IV The positional parameters as P4mm for the hydrothermal $BaTiO_3$ particles with Mg of 0.155 wt%

	g	x	y	z	B
Ba	0.83	0.0000	0.0000	−0.005970	0.19
Ti	0.60	0.5000	0.5000	0.4932	0.35
Mg	0.40	0.5000	0.5000	0.4896	0.45
O(1)	0.54	0.5000	0.5000	0.01549	0.88
O(2)	1.0	0.5000	0.0000	0.5184	0.74

*g: occupation factor; B (Å^2): Isotropic thermal parameter.

TABLE V The positional parameters as Pm3m for hydrothermal $BaTiO_3$ particles with Mg of 0.155 wt%

	g	x	y	z	B
Ba	0.93	0.0000	0.0000	0.0000	0.17
Ti	0.79	0.5000	0.5000	0.5000	0.30
Mg	0.21	0.5000	0.5000	0.5000	0.17
O	0.99	0.5000	0.5000	0.0000	0.99

*g: occupation factor; B (Å^2): Isotropic thermal parameter.

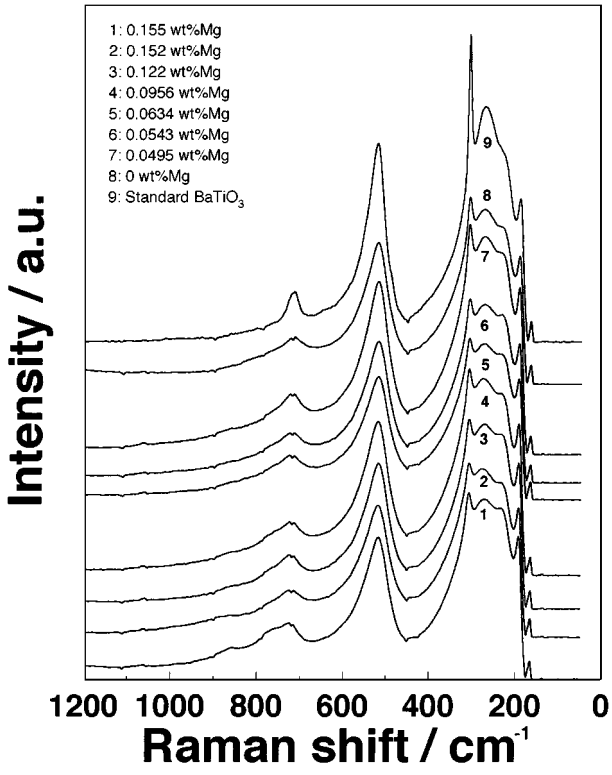

Figure 8 Powder Raman scattering spectra of hydrothermal $BaTiO_3$ particles with various Mg contents treated at 800 °C for 1 h.

$BaTiO_3$ (P4mm) are $4E(TO + LO) + 3A_1(TO + LO) + 1B_1$, while in cubic (Pm3m) there is no Raman-active mode [25]. In Fig. 8, manyRaman peaks were observed, and the most of peaks could be assigned to those of tetragonal $BaTiO_3$. The peaks around 720, 515, 305 and 260 cm^{-1} were assigned to the overlap of $E(4LO) + A_1(3LO)$, $E(4TO) + A_1(3TO)$, $E(3TO) + E(2LO) + B_1$ and $A_1(2TO)$, respectively, on the basis of the assignment reported by Scalabrin *et al.* [26]. But only peak around 870 cm^{-1} can not be assigned. In our recent study, we measured powder Raman spectra of the hydrothermal $BaTiO_3$ particles only with various concentration of hydroxyl group, and found an unknown peak around 810 cm^{-1}, which could not be assigned to phonon modes of $BaTiO_3$ [20]. The peak around 810 cm^{-1} appeared with increasing concentration of the lattice hydroxyl group, and in $BaTiO_3$ particles without lattice hydroxyl group it was not observed. Thus, we assigned the peak to deformation vibration of the lattice hydroxyl group. However, in this study, we also found an unknown peak around 870 cm^{-1}, and this one can not be assigned to phonon mode of MgO. At present, we consider that this peak may be caused by a defect structure formed by an addition of Mg into $BaTiO_3$.

In Fig. 8, the intensities of Raman peaks assigned to P4mm were almost constant despite Mg content, which revealed that a local crystal structure of hydrothermal $BaTiO_3$ particles with various Mg contents was tetragonal. On the other hand, an average crystal structure of hydrothermal $BaTiO_3$ particles estimated using XRD measurement could changed from tetragonal to cubic with increasing Mg content. In $BaTiO_3$ single crystal, Kay and Vousden reported that the average crystal structure from XRD measurements changed drastically from tetragonal to cubic at 120 °C with increasing temperature [3] while many investigators found that the local crystal structure from Raman scattering measurements remained tetragonal above 120 °C [27–33]. This difference indicated that a phase transition of $BaTiO_3$ is not simple displacive-type but complicated displacive-type phase transition with order-disorder behavior. In this study, we could observe that in hydrothermal $BaTiO_3$ particles including Mg, with increasing Mg content, the average crystal structure changed gradually from tetragonal to cubic while the local crystal structure remained tetragonal. This result is similar to the abovementioned behavior of two kinds of crystal structure (i.e., average and local) of $BaTiO_3$ single crystal above Tc. Moreover, in the hydrothermal $BaTiO_3$ particles including lattice hydroxyl group, an observation of the order-disorder behavior similar to that in the hydrothermal $BaTiO_3$ particles including Mg was reported [20]. The above results suggested that the lattice defects induced by an addition of Mg and OH^- into $BaTiO_3$ can cause the order-disorder behavior in the crystal structure of $BaTiO_3$, i.e., these lattice defects can cause the structural phase transition of $BaTiO_3$.

3.3. Analysis of lattice vibration

For the purpose of the analysis of the phonon, we measured the far-infrared reflection spectra (the incident angle of 16 deg.) using only the hydrothermal $BaTiO_3$ particles without the diluents such as KBr and CsI, in addition to powder Raman scattering spectra (Fig. 8). In the far-infrared reflection method using powder-like sample, it is known that specular reflection becomes very weak due to a large ratio of scatting light, and it has ever been difficult to obtain the clear reflection spectra. In this study, we used aluminum fine powders with an average particle size of a few μm as a reference to equalize an intensity of specular reflection from $BaTiO_3$ particles with that from the reference (Al powders). As the result, we could obtain the clear reflection spectra (=solid line), as shown in Fig. 9.

In Fig. 9, as the reference sample, there is a FIR spectrum of standard tetragonal $BaTiO_3$ particles with a tetragonality of 1.011. Raman measurements (Fig. 8) revealed that a symmetry of the hydrothermal $BaTiO_3$ particles with and without Mg was P4mm. In tetragonal $BaTiO_3$ (P4mm), there are seven infrared-active modes, i.e., $3A_1(TO + LO) + 4E(TO + LO)$ modes [34]. Thus, from FIR reflection spectra in Fig. 9, we can do the analysis of the phonon. In general, for the analysis of the phonon, two models had been reported, i.e., (a) a classical damped oscillator model [34] and (b) a Four-Parameter Semi-Quantum (FPSQ) model [35]. The classical damped oscillator model can apply in only the case of well separated infrared bands such as CaF_2, SrF_2 and BaF_2, [36] while the FPSQ model can apply in the case of broad infrared bands such as ferroelectrics [37–40]. In recent study, we analyzed IR reflection spectra of the hydrothermal $BaTiO_3$ particles including lattice hydroxyl group using the FPSQ model, and then could estimate clearly the phonon parameters [20]. Therefore,

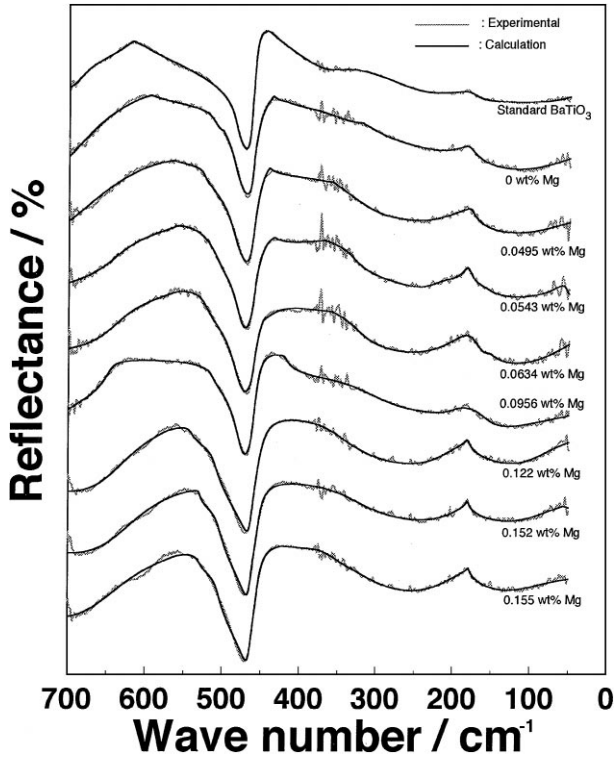

Figure 9 FIR reflection spectra of hydrothermal $BaTiO_3$ particles with various Mg contents treated at 800 °C for 1 h.

in this study, the phonon parameters of the hydrothermal $BaTiO_3$ particles including Mg were also estimated using the FPSQ model.

Here, tetragonal $BaTiO_3$ is an anisotropic crystal, and has the different characteristics along two directions i.e., *a*-axis (=*b*-axis) and *c*-axis. Among some characteristics, it is also well known that the dielectric constant along *a*-axis ($=\varepsilon_a$) is different from that along *c*-axis ($=\varepsilon_c$), i.e., ε_a is much greater than ε_c, as reported by Merz [41]. In the FPSQ model, the complex dielectric constant ($=\varepsilon$) can be expressed as a product of each oscillator with four parameters, i.e., $\omega_{j\mathrm{LO}}$ (resonance frequency of longitudinal optical LO mode), $\gamma_{j\mathrm{LO}}$ (damping factor of LO mode), $\omega_{j\mathrm{TO}}$ (resonance frequency of transverse optical TO mode) and $\gamma_{j\mathrm{TO}}$ (damping factor of TO mode), as shown in Equation 2.

$$\varepsilon = \varepsilon_\infty \prod_j \frac{\omega_{j\mathrm{LO}}^2 - \omega^2 + i\gamma_{j\mathrm{LO}}}{\omega_{j\mathrm{TO}}^2 - \omega^2 + i\gamma_{j\mathrm{TO}}} \tag{2}$$

As above mentioned, there are two kinds of dielectric constants (ε_a and ε_c) in tetragonal $BaTiO_3$. Infrared-active phonon modes along *a*-axis are four E(LO + TO) modes while those along *c*-axis are three A_1(LO + TO) modes. Therefore, ε_a can be expressed as a product of four oscillators while ε_c can be expressed as a product of three oscillators using Equation 2. Moreover, according to the FPSQ model, an infrared reflectivity ($=R$) can be expressed using the complex dielectric constant, as shown in Equation 3.

$$R = \left| \frac{\sqrt{\varepsilon} - 1}{\sqrt{\varepsilon} + 1} \right|^2 \tag{3}$$

Here, the reflectivity calculated from Equation 3 is a physical quantity corresponding to infrared reflectance measured by FIR reflection method. In tetragonal $BaTiO_3$, there are two kinds of reflectivities as the same as the dielectric constants, i.e., R_a and R_c means a reflectivity measured by an incident light parallel to a direction of *a*-axis and *c*-axis, respectively. Thus, R_a and R_c can be obtained by substituting ε_a and ε_c in Equation 3, respectively.

Here, we must make an important assumption as follows. In tetragonal $BaTiO_3$ particles, the directions of the spontaneous polarization of each crystalline are random. Thus, the ratio of the *a*-plane to the *c*-plane perpendicular to the incident light can assume 2 : 1. Using this assumption, the whole infrared reflectivity *R* can be expressed using R_a and R_c, as shown in Equation 4.

$$R = \frac{1}{3}R_c + \frac{2}{3}R_a \tag{4}$$

In the above model, there are 30 phonon parameters. These phonon parameters were adjusted using a nonlinear least squares method with a program SALS [42] until the calculated reflectivities fit the experimental reflectivities. Fitting results using this method are shown as dashed lines in Fig. 9. The fitting results (dashed line) were in excellent agreements with the experimental results (solid line).

By the adjustment using the above nonlinear least squares method, we could obtain 30 phonon parameters, and there were the parameters of the phonon such as E(1TO), A_1(1TO) and A_1(3LO) modes, which can be observed experimentally only in the region below 50 cm^{-1} and above 700 cm^{-1}. However, these three modes could not be measured directly because of the limitation of the equipment. Thus, in order to investigate the state of the phonon, it is a problem to use the calculated phonon parameters in E(1TO), A_1(1TO) and A_1(3LO) modes, and the accuracy of these parameters is also very doubtful. In this study, we used the phonon parameters of the other modes except for E(1TO), A_1(1TO) and A_1(3LO) modes for the analysis of the phonon.

Figs 10 and 11 show the dependence of the resonance frequency for E and A_1 modes estimated from the analysis of FIR reflection spectra on Mg content, respectively. The resonance frequencies of E and A_1 modes were almost constant regardless of Mg contents. On the other hand, Figs 12 and 13 show the dependence of the damping factor for E and A_1 modes estimated from the analysis of FIR reflection spectra on Mg content, respectively. The damping factors of E and A_1 modes increased linearly with increasing Mg contents.

As above mentioned, the phonon parameters can be also estimated from the powder Raman spectra (Fig. 9). In Fig. 9, on the assumption that Raman peak can be expressed as Lorentz resonance curve, as reported by Burns and Scott, [2] we estimated the resonance frequency, which equals to the top of a peak, and the damping factor, which equals to FWHM of the peak. It, however, should be noted that the peaks in Fig. 9 were overlapping peaks of some phonon modes, and could

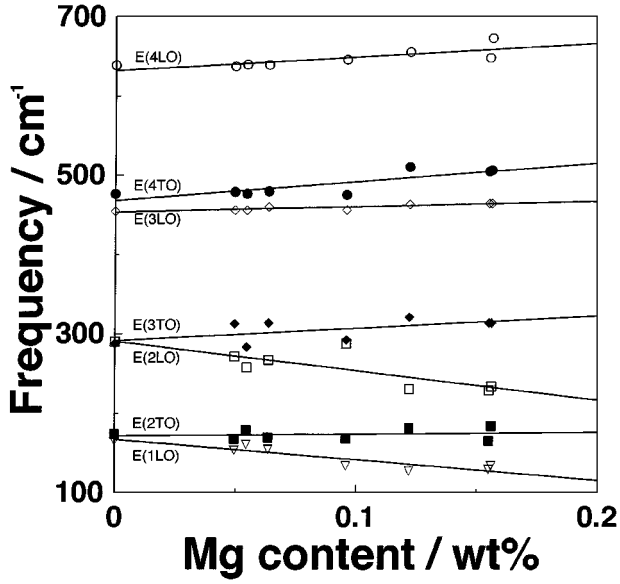

Figure 10 The dependence of the resonance frequency of E modes estimated from the FIR reflection spectra on Mg content in hydrothermal $BaTiO_3$ particles.

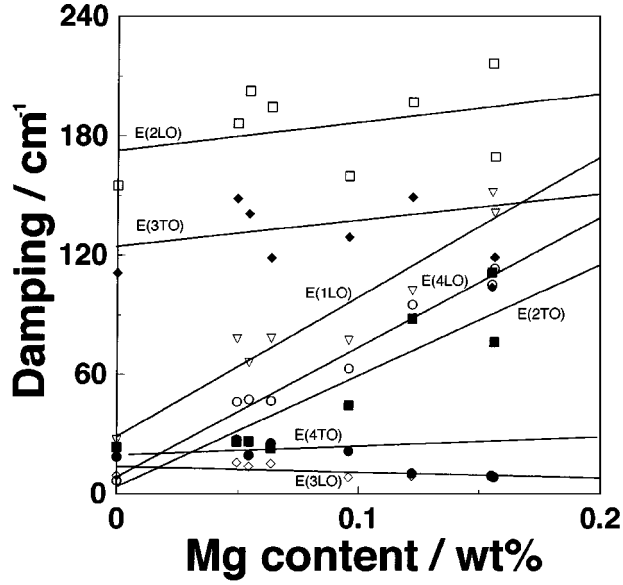

Figure 12 The dependence of the damping factor of E modes estimated from the FIR reflection spectra on Mg content in hydrothermal $BaTiO_3$ particles.

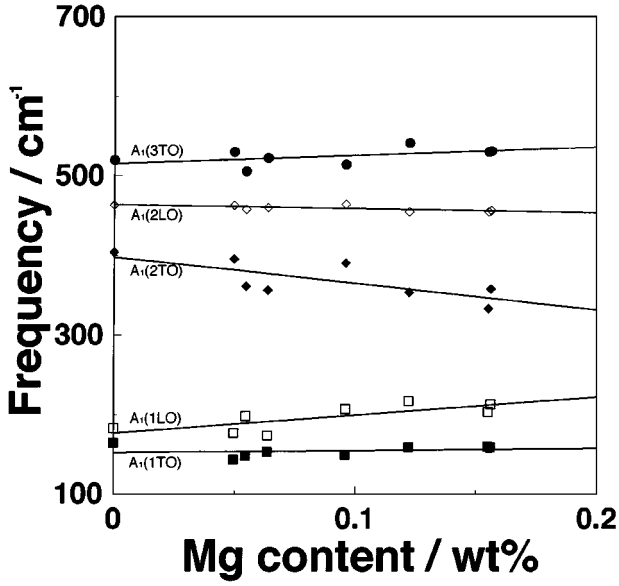

Figure 11 The dependence of the resonance frequency of A_1 modes estimated from the FIR reflection spectra on Mg content in hydrothermal $BaTiO_3$ particles.

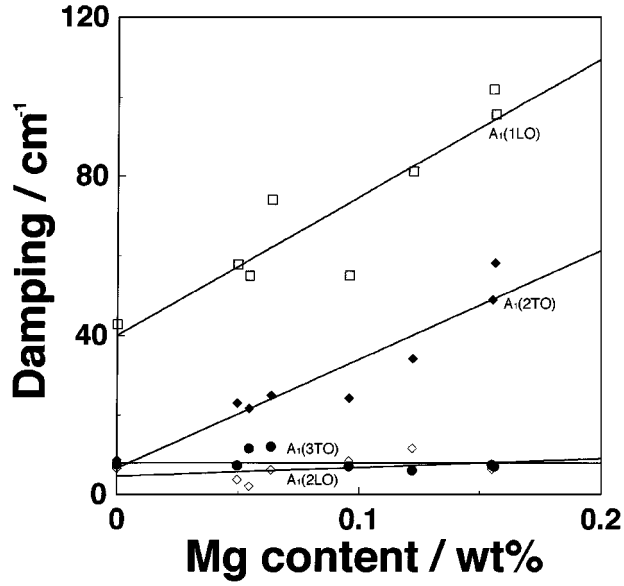

Figure 13 The dependence of the damping factor of A_1 modes estimated from the FIR reflection spectra on Mg content in hydrothermal $BaTiO_3$ particles.

not be separated into each phonon mode. Therefore, a accuracy of the phonon parameters estimated from Fig. 9 is less than those from analysis of FIR spectra, but the tendency of the parameters on Mg contents has high accuracy. Figs 14 and 15 show the dependence of the resonance frequency and the damping factor estimated from the powder Raman spectra on Mg content, respectively. The resonance frequencies of $E + A_1$ modes were almost independent of Mg contents while the damping factors of $E + A_1$ modes increased linearly with increasing Mg content. This result agreed with that obtained from the analysis of FIR spectra. Servoin *et al.* measured the FIR reflection spectra of tetragonal $BaTiO_3$ single crystal at room temperature, and obtained phonon parameters using the FPSQ model [38]. Their calculated resonance frequencies of all $BaTiO_3$ phonon modes agreed almostly with our results while their damping factors were smaller than our results of hydrothermal $BaTiO_3$ particles without Mg.

In hydrothermal $BaTiO_3$ particles including lattice hydroxyl group, we could obtain the results, that the damping factor increased linearly with increasing concentration of lattice hydroxyl group while the resonance frequency was almost constant despite the concentration of lattice hydroxyl group. This tendency agreed almostly with that in the hydrothermal $BaTiO_3$ particles including Mg. Moreover, the phonon parameters of O_6 octahedra deformation mode (=E(4LO), E(4TO), A_1(3LO) and A_1(3TO) modes) in the hydrothermal $BaTiO_3$ particles including lattice hydroxyl group of 0.9 wt% [20] agreed almostly with those in the hydrothermal $BaTiO_3$ particles including Mg of

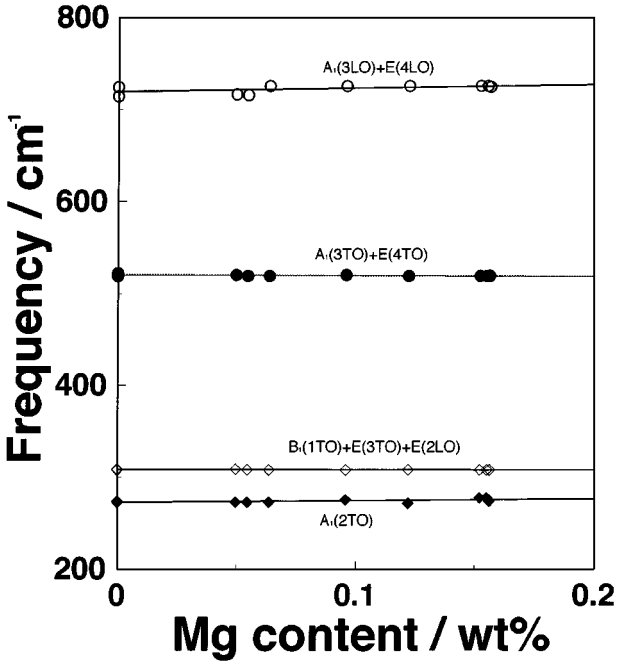

Figure 14 The dependence of the resonance frequency of E and A_1 modes estimated from the powder Raman spectra on Mg content in hydrothermal $BaTiO_3$ particles.

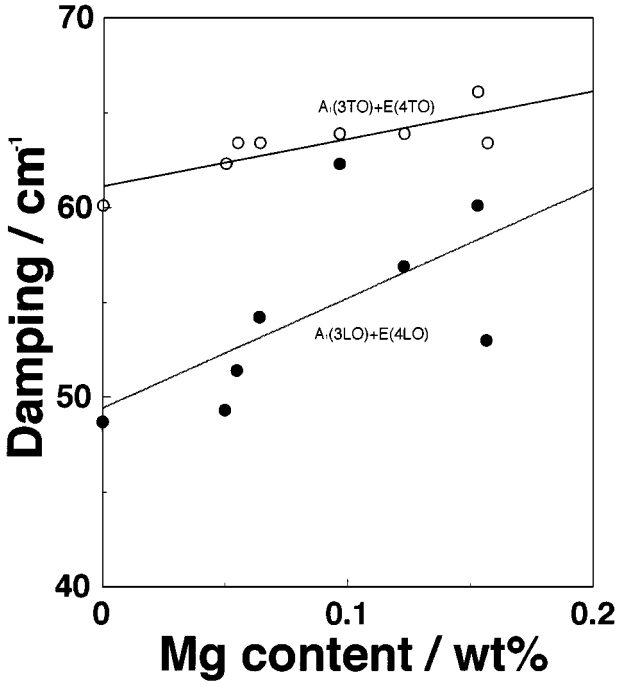

Figure 15 The dependence of the damping factor of E and A_1 modes estimated from the powder Raman spectra on Mg content in hydrothermal $BaTiO_3$ particles.

0.156 wt%. Thus, we believe that the effects of the lattice defects induced by Mg and lattice hydroxyl group on the phonon can be explained using the same mechanism.

4. Discussion

4.1. Dependence of phonon parameters on Mg contents

In this study, we could estimate the phonon parameters using two methods, i.e., powder Raman and FIR reflection spectra. Among the phonon parameters, the resonance frequencies of $A_1(3TO) + E(4TO)$ modes from the powder Raman spectra were about 510 cm^{-1}, and independent of Mg content, while those of the same modes from the FIR reflection spectra also were about 480–510 cm^{-1}, and independent of Mg content. These results indicated that difference between resonance frequencies of the same phonon mode obtained by two methods was present within the error of 5%. This is because the phonon parameters from the powder Raman spectra have an experimental error owing to their overlapping peaks, and those from FIR reflection spectra have a calculation error owing to curve-fitting by the FPSQ model.

On the other hand, the damping factors of $A_1(3TO) + E(4TO)$ modes estimated from the powder Raman spectra increased slightly with increasing Mg contents while a sum of the damping factors of $A_1(3TO)$ and E(4TO) modes from the FIR reflection spectra were almost constant at about 40 cm^{-1} despite Mg contents and was smaller than that of about 60 cm^{-1} from the Raman spectra. Therefore, we think that difference between damping factors of the same phonon mode estimated by two methods was present without the error of measurement and calculation. Moreover, the damping factors of $A_1(3LO) + E(4LO)$ modes from Raman spectra increased slightly from 50 to 60 cm^{-1} with increasing Mg contents while damping factor of only E(4LO) mode from FIR spectra increased largely from 10 to 100 cm^{-1} with increasing Mg contents. These results indicated that the resonance frequencies of $BaTiO_3$ phonon estimated from two methods were almost same while the damping factors from two methods were quite different.

In general, the Raman scattering measurement can give directly the state of the phonon while the IR reflection measurement can give directly the reflective index, and can estimate the state of the phonon from its reflective index using FPSQ model, which means that the phonon parameters from Raman spectra have better accuracy than those from IR reflection spectra. Moreover, in Raman spectra, the change of damping factors of $A_1(3TO) + E(4TO)$ modes was similar to that of $A_1(3LO) + E(4LO)$ modes, which showed that the dependences of both LO and TO modes on Mg contents was similar. But, in the analysis of E(4TO) and E(4LO) modes from FIR spectra, the change of damping factor of TO mode was quite different from that of LO mode.

In $BaTiO_3$ single crystal, Luspin *et al.* reported that the damping factors of TO and LO modes of the same phonon except for a soft mode showed the similar dependencies on temperature [37]. Thus, in this study, the similar dependence of damping factors of both LO and TO modes obtained from Raman measurement on Mg contents was reasonable, but the different dependence of damping factors of LO and TO modes obtained from FIR measurement on Mg contents was abnormal. The above discussion suggested that among the phonon parameters estimated from FIR reflection spectra using the FPSQ model, there may be a certain problem only in a estimation of the damping factor.

Essentially, in order to estimate the phonon parameters from IR reflection spectra, it is necessary to measure a spectrum using an incident and a reflex light normal to the surface (=an incident angle of 0 deg.) [34]. In this study, however, we measured the FIR reflection spectra using an angle of the incidence and the reflection of 16 deg. because of the limitation of the equipment. In our recent study, the IR reflection spectra were measured using an angle of incidence and reflection of 8 deg. In the use of an angle of incidence and reflection of 8 deg, the phonon parameters from IR reflection spectra agreed with those from Raman spectra. Thus, we regarded these spectra (8 deg.) as the same spectra as IR reflection spectra measured using an angle of incidence and reflection of 0 deg. However, it is impossible to regard an angle of incidence and reflection of 16 deg as 0 deg. Therefore, in these FIR reflection spectra (Fig. 9), the contribution of other components except for normal component to the surface was larger, and may not be neglected.

Moreover, Equation 3 is the equation established on the basis of the assumption that only normal component to the surface can be contributed in the reflectivity [34]. Therefore, for the analysis of the FIR reflection spectra measured using an angle of incidence and reflection of 16 deg, it can be a problem to estimate the phonon parameters using the Equation 3. This suggested that the values themselves of phonon parameters obtained from the analysis of FIR reflection spectra were meaningless, but its dependence of these phonon parameters on Mg contents were useful, i.e., the tendency from the FIR measurement, that the resonance frequency was almost constant despite Mg contents while the damping factor increased with increasing Mg content, was useful and agreed with that from the Raman measurement. Thus, in this study, we believe that the dependence of the phonon parameters on Mg contents, which the resonance frequency was almost constant depend Mg contents while the damping factor increased with increasing Mg content, was correct.

4.2. Difference between local and average crystal structure of $BaTiO_3$ including Mg

In this study, we observed an average crystal structure of the hydrothermal $BaTiO_3$ particles including Mg using a XRD measurement while observed its local crystal structure using a Raman and a FIR measurements. The refinement of the average crystal structure by the Rietveld method showed that the average crystal structure of the hydrothermal $BaTiO_3$ particles without Mg was the tetragonal with a c/a ratio of 1.00154, and the average crystal structure of hydrothermal $BaTiO_3$ particles including Mg of 0.155 wt% was the cubic. Moreover, XRD measurement of a (200) plane of $BaTiO_3$ indicated that the tetragonality of the tetragonal structure decreased linearly with increasing Mg contents. On the other hand, the powder Raman and the FIR measurements revealed that the local crystal structure of the hydrothermal $BaTiO_3$ particles was the tetragonal despite Mg contents, and Raman intensity was also independent of Mg contents.

This result showed that with increasing Mg contents, the average crystal structure of the hydrothermal $BaTiO_3$ particles approached from the tetragonal to the cubic while their local crystal structure remained the tetragonal. In our recent study, we could report that in the hydrothermal $BaTiO_3$ particles including lattice hydroxyl group, with increasing concentration of lattice hydroxyl group, the average crystal structure of the hydrothermal $BaTiO_3$ particles became from the tetragonal to the cubic while their local crystal structure remained the tetragonal [20]. These results suggested that in the crystal structure of $BaTiO_3$ particles, the lattice defects induced by lattice hydroxyl group or Mg can cause an order-disorder behavior, which the local crystal structure is the tetragonal while the average crystal structure is the cubic, i.e., the polar direction of each tetragonal unit cell is flipping by the thermal energy of kT (k and T is Boltzmann constant and room temperature, respectively).

These confirmation of the order-disorder behavior is found for the first time in the crystal structure of $BaTiO_3$ particles, but in large $BaTiO_3$ single crystal, some investigations have already reported the similar behaviors above Tc [27–33, 43–46]. In $BaTiO_3$ single crystal, it has been well known that above Tc, there was the order-disorder behavior, which the average crystal structure from the XRD measurements was the cubic while the local crystal structure from Raman measurement was not the cubic phase. This indicated that the order-disorder behavior in the crystal structure was an intrinsic characteristic of $BaTiO_3$ above Tc.

In this study, the lattice defect induced by Mg in $BaTiO_3$ particles caused the order-disorder behavior into the crystal structure at room temperature, which suggested that this lattice defect made the average and local crystal structures of $BaTiO_3$ particles at room temperature the similar ones to the crystal structure of large $BaTiO_3$ single crystal above Tc. Why could the lattice defect affect the crystal structure of $BaTiO_3$ particles? We will discuss about this question in the following section.

4.3. Role of lattice defect introduced by Mg on phonon and crystal structure

Generally, the introduction of a lattice defect into an ideal crystal can result in the formation of a mass and a spring constant quite different from intrinsic those of the ideal crystal in its phonon, considering the phonon behavior using the Einstein model. Thus, it can be expected that the kinetic and potential energies in the surroundings of the lattice defect are quite different from those in a part without defect [47]. In other words, the phonon parameters such as the damping factor, the oscillation strength and the resonance frequency, which can express the state of the phonon, can also change near the defect.

In this study, the lattice with Mg ion substituted in the position of Ti ion of a $BaTiO_3$ lattice can have a lighter mass than that of the defect-free $BaTiO_3$ lattice. This is because a mass of Mg (=24.3 g/mol) is much lighter than that of Ti (=47.9 g/mol). Moreover, the

substitutional Mg ion can also form a weaker spring constant, i.e., make much weaker Coulomb attractive forces of Mg-O than that of Ti-O. This is because (a) a fractional ionic character in Mg-O bond was greater than that in Ti-O bond owing to a smaller electronegativity of Mg (=1.2) than that of Ti (=1.5), and (b) a charge number of Mg (=+2) was much smaller than that of Ti (=+4). Thus, it can be expected that a vibration energy (=resonance frequency) of the $BaMgO_2$ lattice including a Mg ion and an oxygen vacancy is quite different from that of the $BaTiO_3$ lattice without defect. However, the resonance frequencies of all phonon modes estimated from Raman and FIR in this study were almost independent of Mg contents, as shown in Figs 10, 11 and 14, and were almost similar values to those obtained in $BaTiO_3$ single crystal without defect, which indicated that although $BaMgO_2$ lattice including a Mg ion and an oxygen vacancy has the resonance frequencies different from those without defect, the $BaMgO_2$ lattice must vibrate really at the resonance frequencies equivalent to those without defect. This means that in order to make the lattice including a Mg ion and an oxygen vacancy vibrate at the resonance frequencies equivalent to those without defect, an excess energy corresponding to the difference between vibration energies of the lattice with and without defects is required. As the result, the substitutional Mg ion can act as a resister in all phonon of $BaTiO_3$, [34] e.g., the O_6 octahedra deformation mode, silent mode (=O_4 torsional mode), Last mode (=Ba-TiO_6 translational mode) and Slater mode (=Ti-O_6 translational mode). These modes lose gradually its vibration energy near the defect, and thus the life time of these phonon becomes shorter, i.e., its damping factor increases. The increase of the damping factor can make the state of the phonon very unstable, which means that the lattice defect can give the influence similar to the increase of temperature on the crystal structure of $BaTiO_3$, as reported by Luspin *et al.* [37].

As mentioned above, $BaTiO_3$ has intrinsically the phase transition with an order-disorder behavior as well as well-known displacive behavior at 130 °C, and the lattice defect such as a Mg ion substituted in the position of Ti can enhance the vibration energy at room temperature up to that of pure $BaTiO_3$ above Tc. The hydrothermal $BaTiO_3$ particles including Mg of 0.155 wt% can have very unstable phonon corresponding to that of pure $BaTiO_3$ single crystal above Tc, owing to the presence of higher Mg contents, while the hydrothermal $BaTiO_3$ particles without Mg very stable phonon corresponding to that of pure $BaTiO_3$ single crystal below Tc.

Therefore, the crystal structure of the hydrothermal $BaTiO_3$ fine particles with high Mg contents becomes to cubic or tetragonal with a small tetragonality. The above discussion could be applied on the occasion of the hydrothermal $BaTiO_3$ fine particles with high concentration of lattice hydroxyl group. This suggests that the effect of the lattice defect on the phonon and the crystal structure can be explained using the same mechanism despite the kinds of the lattice defects. Therefore, in order to predict the effect of lattice defect on the phonon and the crystal structure of $BaTiO_3$, it is very important to estimate the difference between the vibration energies of the $BaTiO_3$ lattices with and without lattice defects. In our model, it can be expected that as this difference between the vibration energies of two state increases, the influence of the lattice defects on the phonon and the crystal structure also can increase. Thus, we will discuss about the effects of Mg ion and lattice hydroxyl group on the phonon and the crystal structure of hydrothermal $BaTiO_3$ fine particles in the next section.

4.4. Modification in definition of the correlational size of dipole

In the recent study, we proposed the correlational size of dipoles as one of the physical quantities which can express a propagation length of a phonon, i.e., a mean free path of a phonon, because a phonon is a damped oscillation [19]. In an ideal single crystal, which is defect-free and enough large, there is a maximum mean free path of a phonon (=S_t) at certain temperature (in general, it is known that S_t at room temperature can be a couple nm). However, in the single crystal with the lattice defects, on the assumption that these defects are the point defects and have the uniform and random distribution in the crystal, a distance between neighboring defects becomes shorter with increasing number of the lattice defects. As above mentioned, in the surroundings of the lattice defects, a phonon loses its vibration energy, i.e., one ideal phonon can be disturbed near the lattice defects. We defined this distance between neighboring lattice defects as the correlational size of dipoles (=S). Fig. 16 shows a one-dimensional model of the correlational size of dipoles. In the occasion of $S_t < S$, the state of a phonon is almost similar to that of an ideal single crystal, but if $S_t \approx S$ or $S_t > S$, the state of a phonon can change significantly to unstable state, and the state of a phonon becomes more unstable with decreasing S.

In the hydrothermal $BaTiO_3$ fine particles with high concentration of lattice hydroxyl group, we could explain the role of lattice hydroxyl group using this model, and defined S, as shown in Equation 5.

$$S \fallingdotseq \left(\frac{V}{n}\right)^{1/3} \tag{5}$$

Where V is a unit mol volume of $BaTiO_3$ (V: 38.74 cm^3/mol), and n is the number of the lattice defects involved in V. But, Equation 5 means that S can be depend on only the number of the lattice defects, and is independent of other factor. Thus, Equation 5 suggests

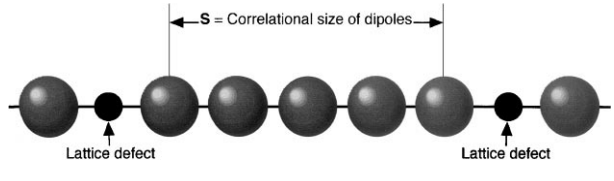

Figure 16 A one-dimensional model of the correlational size of dipoles (=S).

that the correlational size of dipoles S is independent of the kinds of the lattice defects.

In this and recent studies, [20] with increasing concentration of the lattice defects, the phonon became more unstable and the average crystal structure changed from tetragonal to cubic. However, there was a large difference between the effects of Mg and lattice hydroxyl group on the phonon and the crystal structure of $BaTiO_3$. In fact, when with increasing concentration of the lattice defects, a damping factor of E(4LO) mode increased to about 120 cm^{-1}, the average crystal structure was assigned to cubic from the Rietveld method, and FWHM of a (200) plane decreased to about 4×10^{-3} rad, there was lattice hydroxyl group of about 0.9 wt% as H_2O in the hydrothermal $BaTiO_3$ fine particles (62.5 nm) including lattice hydroxyl group while there were Mg of about 0.15 wt% in hydrothermal $BaTiO_3$ fine particles (63.1 nm) including Mg.

In the hydrothermal $BaTiO_3$ fine particles including lattice hydroxyl group of 0.9 wt% as H_2O, there is one substitutional lattice hydroxyl group in 13 lattice oxygen sites, i.e., there is one lattice hydroxyl group in four $BaTiO_3$ lattices, while in hydrothermal $BaTiO_3$ fine particles including Mg of 0.15 wt%, there is one substitutional Mg ion in 70 Ti sites, i.e., there is one Mg in 70 $BaTiO_3$ lattices. Here, each correlational size of dipoles in hydrothermal $BaTiO_3$ particles including lattice hydroxyl group of 0.9 wt% as H_2O and Mg of 0.15 wt% estimated using Equation 5 is 0.63–0.80 nm and 1.65 nm, respectively. This result indicated that in order to give the same effect on the phonon and the average crystal structure of hydrothermal $BaTiO_3$ particles, the correlational size of dipoles in $BaTiO_3$ particles including Mg was about twice longer than that in $BaTiO_3$ particles including lattice hydroxyl group. Therefore, it is necessary for the correlational size of dipoles to consider about an influence of the kinds of lattice defects, and it is much important to redefine the correlational size of dipoles considering the kinds of lattice defects.

In order to correct the different correlational sizes of dipoles by the kinds of the lattice defects, a normalization of the correlational size of dipoles is necessary. Here, it must be considered that what physical quantity can be affected by the lattice defects. As mentioned above, the lattice defect can act as a resister in the $BaTiO_3$ phonon. This is because a vibration energy in the $BaTiO_3$ lattice without defect is quite different from that in the $BaTiO_3$ lattice with defects. At present, we think that as the difference between vibration energies in the $BaTiO_3$ lattices with and without defect becomes larger, the effect of the defect on the phonon and the average crystal structure of $BaTiO_3$ particles also becomes larger. Thus, in order to correct the difference of the kinds of the lattice defects, we propose a new constant, O_i (i: the kinds of the lattice defect), in the redefinition of the correlational size of dipoles S' on the basis of the difference between vibration energies in the $BaTiO_3$ lattices with and without defect, as shown in Equation 6.

$$S' \propto O_i \left(\frac{V}{n}\right)^{1/3} \tag{6}$$

Here, O_i is assumed to be inversely proportional to the magnitude of the difference between vibration energies in the $BaTiO_3$ lattices with and without defect, which means that as the difference between vibration energies in the $BaTiO_3$ lattices with and without defect becomes larger, O_i becomes smaller, i.e., S' becomes smaller while as the difference becomes smaller, O_i becomes larger, i.e., S' becomes larger.

On the occasion of a use of Equation 5, S in the hydrothermal $BaTiO_3$ particles including Mg and lattice hydroxyl group is 1.65 nm and 0.63–0.80 nm, respectively. In this case ($S_{OH} = 0.63$–0.80 nm and $S_{Mg} = 1.65$ nm), the additive effect of Mg and lattice hydroxyl group on the phonon and the average crystal structure of $BaTiO_3$ can became almost same. Therefore, for $S'_{OH} \approx S'_{Mg}$, a ratio of O_{OH} to O_{Mg} must become about 2.0–2.6 in Equation 6. This value is an experimental result, and in order to prove this concept, it is necessary to calculate the difference between vibration energies in the $BaTiO_3$ lattices with and without defect using a Molecular Mechanics method, e.g., a calculation of the difference between vibration energies in the pure $BaTiO_3$ lattices and the pure $BaMgO_2$ lattices, where there are a substitutional Mg ion and an oxygen vacancy in a $BaTiO_3$ lattice, and confirm that a ratio of a vibration energy in the $BaTiO_3$ lattice including 0.9 wt% as H_2O to that in $BaTiO_3$ lattice including Mg of 0.15 wt% becomes about 2. But, the normalization using Equation 6 was introduced only for the purpose of the correction of the different correlational sizes of dipoles by the kinds of the lattice defects, and S' was meaningless itself.

On the basis of the above discussion, in order to study the state of the phonon, it is most important to estimate a mean free path of a phonon. After this, using a measurement of a thermal conductivity, it will be possible to estimate the mean free path of a phonon. Moreover, we believe that the effect of the lattice defect on the crystal structure of $BaTiO_3$ can be also explained using the modified soft-mode theory, and thus it will be much important to detect directly and analyze the soft mode (=Slater mode) in the hydrothermal fine $BaTiO_3$ particles.

5. Conclusion

$BaTiO_3$ fine particles with various Mg contents were prepared by the hydrothermal method. TEM observation showed that these particles were spherical single crystallites of $BaTiO_3$ with an average size of about 63 nm regardless of Mg contents. AA and ICP-MS indicated that Mg contents included in the particles could be controlled in the range from 0 to about 0.15 wt%, and moreover, an impedance spectroscopy revealed that the resistance of intraparticle decreased with increasing Mg content. On the basis of the results, it was confirmed that Mg replaced substitutionally on Ti site in a $BaTiO_3$ lattice. As a result of a XRD measurement, an average crystal structure of the particles without Mg was tetragonal with a tetragonality of 1.0015 while the average crystal structure approached to cubic gradually with increasing Mg content. On the other hand,

a Raman measurement indicated that the local crystal structure was tetragonal regardless of Mg contents. This suggested that there was order-disorder behavior in the crystal structure of hydrothermal $BaTiO_3$ particles including Mg of 0.155 wt%. The similar order-disorder behavior was observed in the crystal structure of hydrothermal $BaTiO_3$ particles including lattice hydroxyl group of 0.9 wt% as H_2O, and in the crystal structure of $BaTiO_3$ single crystal above Tc. Thus, we believe that the order-disorder behavior in the crystal structure of the hydrothermal $BaTiO_3$ particles was intrinsic characteristics of $BaTiO_3$, and the lattice defects could make this order-disorder behavior in the crystal structure occur.

Moreover, Raman and IR spectra showed that resonance frequency for each phonon mode was independent of Mg contents while their damping factor increased with increasing Mg content, which suggested that state of the phonon became unstable with increasing Mg content. Thus, we discussed about the additive effect of Mg on the crystal structure of hydrothermal $BaTiO_3$ particles, based on the stability of phonon. As a result, we found that the lattice defects introduced by Mg into $BaTiO_3$ lattices can act as resister on the $BaTiO_3$ phonon, and then a life time of phonon was shorter with increasing Mg content. This suggested that the additive effect of Mg into hydrothermal $BaTiO_3$ particles was the almost similar effect as the increasing temperature in $BaTiO_3$ single crystal.

At last, we modified the definition of the correlational size of dipoles considering the kinds of lattice defects, and proposed a new constant. In order to prove this concept, we will calculate the difference between vibration energies in the $BaTiO_3$ lattices with and without defect using a Molecular Mechanics method.

Acknowledgements

We thank Mr. Sato of Perkin Elmer for kindly allowing us the use of FT-FIR equipment, and associate professor Naoi of Tokyo University of Agriculture and Technology for kindly allowing us the use of Raman scattering equipment. We thank both Mr. Yamada and Ms. Yamanoi of MAC Science for discussing about the crystal structure using the Rietveld method. We also thank both Mr. Yukinari and Mr. Ohkita of Yokogawa Analytical Systems for discussing about elemental analysis. Moreover, this work was partly supported by Grants-in-Aid for Scientific Research (07750009 and 10750488) from the Ministry of Education, Science and Culture.

References

1. G. BURNS and B. A. SCOTT, *Phys. Rev. Lett.* **25** (1970) 167.
2. *Idem., Phys. Rev. B* **7** (1973) 3088.
3. H. F. KAY and P. VOUSDN, *Phil. Mag.* **40** (1949) 1019.
4. A. F. DEVONSHIRE, *ibid.* **40** (1949) 1040.
5. *Idem., ibid.* **42** (1951) 1065.
6. G. A. SAMARA, *Phys. Rev.* **151** (1966) 378.
7. K. ISHIKAWA, K. YOSHIKAWA and N. OKADA, *Phys. Rev. B* **37** (1988) 5852.
8. K. UCHINO, E. SADANAGA and T. HIROSE, *J. Am. Ceram. Soc.* **72** (1989) 1555.
9. K. UCHINO, E. SADANAGA, K. OONISHI, T. MOROHASHI and H. YAMAMURA, "Ceramic Dielectrics; Ceramic Transactions, Vol. 8," (*Am. Ceram. Soc.*, 1990) p. 107.
10. G. ARLT, D. HENNINGS and G. DE WITH, *J. Appl. Phys.* **58** (1985) 1619.
11. W. COCHRAN, *Phys. Rev. Lett.* **3** (1959) 412.
12. *Idem., Adv. in Phys.* **9** (1960) 387.
13. *Idem., ibid.* **10** (1961) 401.
14. T. NAKAMURA, T. SAKUDO, Y. ISHIBASHI and Y. TOMINAGA, "Ferroelectricity involved in Structural Phase Transition" (Shokabo, Tokyo, 1988), in Japanese.
15. R. VIVEKANANDAN, S. PHILIP and T. R. N. KUTTY, *Mater. Res. Bull.* **22** (1986) 99.
16. D. HENNINGS and S. SCHREINMACHER, *J. Eur. Ceram. Soc.* **9** (1992) 41.
17. S. WADA, T. SUZUKI and T. NOMA, *J. Ceram. Soc. Jpn.* **103** (1995) 1220.
18. *Idem., Jpn. J. Appl. Phys.* **34** (1995) 5368.
19. *Idem., J. Ceram. Soc. Jpn.* **104** (1996) 383.
20. T. NOMA, S. WADA, M. YANO and T. SUZUKI, *J. Appl. Phys.* **80** (1996) 5223.
21. B. JAFFE, W. R. COOK and H. JAFFE, "Piezoelectric Ceramics" (Academic Press, New York, 1971) p. 91.
22. M. KLEITZ, H. BERNARD, E. FERNANDEZ and E. SCHOULER, in "Science and Technology of Zirconia," edited by H. HEUER and L. W. HOBBS (Am. Ceram. Soc., 1981) p. 310.
23. B. D. CULLITY, "Elements of X-Ray Diffraction" (Addison-Wesley, Massachusetts, 1980).
24. F. IZUMI, in "Rietveld Method," edited by R. A. YOUNG (Oxford University Press, Oxford, 1993) Ch. 13.
25. G. BURNS, "Introduction to Group Theory with Applications" (Academic Press, New York, 1977), in Japanese.
26. A. SCALABRIN, A. S. CHAVES, D. S. SHIN and S. P. S. PORTO, *Phys. Stat. Sol. B* **79** (1977) 731.
27. J. L. PARSON and L. RIMAI, *Solid State Comm.* **5** (1967) 423.
28. M. DIDOMENICO, S. H. WEMPLE, S. P. S. PORTO and R. P. BAUMAN, *Phys. Rev.* **174** (1968) 522.
29. M. P. FONTANA and M. LAMBERT, *Solid State Comm.* **10** (1972) 1.
30. A. M. QUITTET and M. LAMBERT, *ibid.* **12** (1973) 1053.
31. G. BURNS and F. H. DACOL, *Phys. Rev. B* **18** (1978) 5750.
32. B. JANNOT, L. GNININVI and G. GODEFROY, *Ferroelectrics* **37** (1981) 669.
33. J. A. SANJURJO and R. S. KATIYAR, *ibid.* **37** (1981) 693.
34. G. BURNS, "Solid State Physics, Vol. 4," (Academic Press, Tokyo, 1985).
35. F. GERVAIS and B. PIRIOU, *Phys. Rev. B* **10** (1974) 1642; *ibid., J. Phys. C: Solid State Phys.* **7** (1974) 2374.
36. W. KAISER, W. G. SPITZER, R. H. KAISER and L. E. HOWARTH, *Phys. Rev.* **127** (1962) 1950.
37. Y. LUSPIN, J. L. SERVOIN and F. GERVAIS, *J. Phys. C: Solid State Phys.* **13** (1980) 3761.
38. J. L. SERVOIN, F. GERVAIS, A. M. QUITTET and Y. LUSPIN, *Phys. Rev. B* **21** (1980) 2038.
39. D. A. SAGALA and S. KOYASU, *J. Am. Ceram. Soc.* **76** (1933) 2433.
40. K. FUKUDA, R. KITOH and I. AWAI, *ibid.* **77** (1994) 149.
41. W. J. MERZ, *Phys. Rev.* **76** (1949) 1221.
42. T. NAKAGAWA and Y. OYANAGI, in "Recent Developments in Statistical Inference and Data Analysis," edited by K. MATUSITA (North-Holland, Amsterdam, 1980) p. 221, in Japanese.
43. Y. YAMADA, G. SHIRANE and A. LINZ, *Phys. Rev.* **177** (1969) 848.
44. R. COMES, M. LAMBERT and A. GUINIER, *Solid State Comm.* **6** (1968) 715.
45. G. HONJO, S. KODERA and N. KITAMURA, *J. Phys. Soc. Jpn.* **19** (1964) 351.
46. G. BURNS and F. H. DACOL, *Ferroelectrics* **37** (1981) 661.
47. K. KUDO, "Optical Properties of Materials," 2nd ed. (Ohmu Press, Tokyo, 1990) p. 298, in Japanese.

Received 19 May 1999
and accepted 3 February 2000